# Transverse NMR Relaxation as a Probe of Mesoscopic Structure

Valerij G. Kiselev[1,*] and Dmitry S. Novikov[2]

[1]*Section of Medical Physics, University Hospital Freiburg, D79106 Freiburg, Germany*
[2]*Department of Physics, Massachusetts Institute of Technology, Cambridge, Massachusetts 02139*

(Received 22 January 2002; published 20 December 2002)

Transverse NMR relaxation in a macroscopic sample is shown to be extremely sensitive to the structure of mesoscopic magnetic susceptibility variations. Such a sensitivity is proposed as a novel kind of contrast in the NMR measurements. For suspensions of arbitrary-shaped paramagnetic objects, the transverse relaxation is found in the case of a small dephasing effect of an individual object. Strong relaxation rate dependence on the objects' shape agrees with experiments on whole blood. Demonstrated structure sensitivity is a generic effect that arises in NMR relaxation in porous media, biological systems, as well as in kinetics of diffusion limited reactions.

DOI: 10.1103/PhysRevLett.89.278101 PACS numbers: 87.61.–c, 76.60.Jx, 82.56.Lz

NMR as a structure probe is utilized in the fields as diverse as chemistry, materials science, geology, and biomedicine. Pristine specimens found in Nature, such as rocks or biological tissues, possess a complex structure at a mesocopic scale. This structure is of primary interest in numerous applications. For example, rock porosity in geology is important to assess the oil basin quality. In biological tissues the mesoscopic scale is set by the size of cells and blood vessels whose properties carry significant diagnostic and physiological information.

It is the NMR monitored *diffusion* that is commonly accepted as a probe of mesoscopic structure in both inorganic [1] and living [2,3] specimens. In the present Letter we propose a *magnetic susceptibility contrast* as a structure probe. Susceptibility inhomogeneities are often connected to the geometric structure, such as pore walls in porous media. In biological tissues they are brought by paramagnetic cells, such as deoxygenated red blood cells (RBCs) and iron-enriched cells in the brain gray matter. In some cases the susceptibility contrast can be artificially manipulated.

Below we consider the NMR signal from a suspension of arbitrarily shaped weakly paramagnetic objects. We demonstrate a significant individual object shape dependence of the transverse relaxation rate. We discuss this result in the biomedical context. Applications of the biomedical NMR imaging (MRI) are limited by a spatial resolution $\sim$1 mm, which is larger than the cell size by 2–3 orders of magnitude. Direct resolution enhancement is unfeasible since today MRI hardware hits physiological limits. Our results suggest that further progress can be made by a deeper analysis of the NMR signal since it contains significant information about the paramagnetic tissue structure at the scale of several $\mu$m.

We compare our results with experiments on whole blood [4–6], with the objects being paramagnetic RBCs. Previous theoretical efforts in this context were focused on the effect of paramagnetic inclusions of specific geometries (spheres [7,8] or cylinders simulating blood vessels [7,9,10]). The effect of object shape was not studied theoretically although experiments [11,12] and the Monte Carlo simulation [12] indicate a strong shape dependence of the transverse relaxation.

We model the medium by a suspension of $N \gg 1$ identical mesoscopic paramagnetic objects which are randomly placed and oriented. The NMR signal is acquired from nuclear spins that freely diffuse in the solvent and in the objects. A macroscopic volume $V$ of the suspension is characterized by the volume fraction $\zeta = Nv_0/V$ of objects ($v_0$ = single object's volume). The case of different object species is easily accounted for when $\zeta \ll 1$, since they contribute additively to the relaxation rate [7,9].

Transverse relaxation occurs due to two different mechanisms: (i) microscopic spin-spin interactions at the molecular level and (ii) diffusion of spins in the magnetic field induced by mesoscopic objects. Fast processes (i) average out to produce a monoexponential relaxation. Processes (ii) are described in terms of the transverse magnetization density $\psi(\mathbf{r})$, which evolves due to molecular diffusion and spin precession with the local Larmor frequency varying in space. It obeys the Bloch-Torrey equation [13]

$$\frac{\partial \psi}{\partial t} = \left( D\nabla^2 - \frac{1}{T_2} - i\omega_L - i\omega(\mathbf{r}) \right)\psi, \qquad (1)$$

where $D$ is the diffusion coefficient of the molecules that carry spins and $T_2$ is the relaxation time due to the microscopic interactions. The relaxation rate $1/T_2$ is insensitive to magnetic field inhomogeneities at the mesoscopic scale. Rather, it characterizes local chemical composition. We assume that $D$ and $T_2$ are the same inside the objects and in the solvent. The constant term $\omega_L$ provides the Larmor precession in the homogeneous main field, and $\omega(\mathbf{r}) = \sum_{n=1}^{N} \omega_0(\mathbf{r} - \mathbf{r}_n)$ is the deviation from $\omega_L$ due to the local magnetic fields induced by randomly located paramagnetic objects (as described later).

  

The signal $S(t)$ from a macroscopic sample is the sum of all spin magnetic moments regardless of their initial positions and their Brownian trajectories after the excitation [9]. In terms of the Green's function $\psi(\mathbf{r}, \mathbf{r}_0, t)$ of (1), defined by the initial condition $\psi(\mathbf{r}_0, \mathbf{r}, t = 0) = \delta(\mathbf{r} - \mathbf{r}_0)$,

$$S(t) = \frac{1}{V}\int d^3\mathbf{r} d^3\mathbf{r}_0 \psi(\mathbf{r}, \mathbf{r}_0, t) \equiv e^{-i\omega_L t - t/T_2} s(t). \quad (2)$$

Microscopic processes decouple due to Eq. (1): $\psi = e^{-i\omega_L t - t/T_2}\phi$, with $\phi(\mathbf{r}, \mathbf{r}_0, t)$ accumulating *mesoscopic* effects. The corresponding signal attenuation factor

$$s(t) = \frac{1}{V}\int d^3\mathbf{r} d^3\mathbf{r}_0 \phi(\mathbf{r}, \mathbf{r}_0, t), \qquad s(0) = 1; \quad (3)$$

describing these effects is the main object of our focus.

Consider the mesoscopic part $M(\mathbf{r}_0, t) = \int d^3\mathbf{r}\phi(\mathbf{r}_0, \mathbf{r}, t)$ of the spin packet magnetization. The $d^3\mathbf{r}_0$ integration in (3) effectively averages $M(\mathbf{r}_0, t)$ over randomly positioned objects. For $\zeta \ll 1$, $M$ is a product of factors contributed by individual objects [9]. In this case $s(t)$ is expressible in terms of a *single* object dephasing effect $f(t)$ [7,9]:

$$s = e^{-\zeta f}, \qquad f(t) = \left\langle \int \frac{d^3\mathbf{r}_0}{v_0}\left(1 - \int d^3\mathbf{r}\,\eta(\mathbf{r}_0, \mathbf{r}, t)\right)\right\rangle_o. \quad (4)$$

Here $\eta$ is the mesoscopic part of the spin packet magnetization density in the presence of a single object,

$$\frac{\partial \eta}{\partial t} = [D\nabla^2 - i\omega_0(\mathbf{r})]\eta, \qquad \eta(\mathbf{r}_0, \mathbf{r}, t = 0) = \delta(\mathbf{r} - \mathbf{r}_0), \quad (5)$$

and average $\langle\rangle_o$ in (4) is taken over the object's orientations.

In the main field $B_0\hat{\mathbf{z}}$ each paramagnetic object induces a local Larmor frequency shift $\omega_0(\mathbf{r})$ that is determined by the object's *susceptibility profile* $\chi(\mathbf{r})$. Below we use uniformly magnetized objects to compare with experiments: $\chi(\mathbf{r}) = \chi \cdot v(\mathbf{r})$, $\chi \ll 1$, where $v(\mathbf{r})$ is a shape function: $v = 1$ inside and $v = 0$ outside the object. A convolution in $\mathbf{r}$, $\omega_0$ in the Fourier space is

$$\omega_0(\mathbf{k}) = \delta\omega \cdot Y(\hat{\mathbf{k}}) \cdot \tilde{v}(\mathbf{k}), \qquad \delta\omega = 4\pi\chi\omega_L, \quad (6)$$

where $Y(\hat{\mathbf{k}}) = 1/3 - k_z^2/k^2$ is the longitudinal projection of an elementary magnetic dipole field, and the object's form factor $\tilde{v}(\mathbf{k})$ is the Fourier transform of $v(\mathbf{r})$.

Transverse relaxation is qualitatively different in the limits of strong and weak dephasing. Introduce effective object radius $\rho$ as that of a sphere of a volume $v_0$. Water molecules pass by the object during the diffusion time

$$t_D = \frac{\rho^2}{D}, \quad \text{where } \frac{4}{3}\pi\rho^3 \equiv v_0 = \int d^3\mathbf{r} v(\mathbf{r}). \quad (7)$$

The typical phase acquired by the spins is $\delta\omega \cdot t_D$. In the present work we focus on a weak dephasing case $\delta\omega \cdot t_D \ll 1$ (diffusion narrowing regime). This regime covers a variety of experiments, in particular, spin dephasing in diamagnetic and paramagnetic samples in the field $B_0 \lesssim 1$ T.

We find the Green's function $\eta$ of Eq. (5) perturbatively in the small parameter $\delta\omega \cdot t_D$, and use Eq. (4) to obtain $f(t)$. This approach is analogous to the Born series for the quantum mechanical scattering amplitude.

The zeroth order in $\delta\omega \cdot t_D$ describes free diffusion. In this case the total magnetization of each spin packet is conserved, $\int d^3\mathbf{r}\,\eta(\mathbf{r}_0, \mathbf{r}; t) = 1$ in (4), and $s(t) = 1$. The first order correction to $f$ vanishes since it is proportional to the angular average of the dipole field. The expression for $f$ is dominated by the second order in $\delta\omega \cdot t_D$ (Fig. 1):

$$f(\tau) = \frac{2\pi\alpha^2}{15}\int_0^\infty \frac{dq}{q^2} g(q^2\tau) \int \frac{d\hat{\mathbf{q}}}{4\pi}\left|\frac{\tilde{v}(\mathbf{q})}{\tilde{v}(\mathbf{0})}\right|^2, \quad (8)$$

$$\alpha \equiv \frac{2}{3\pi}\delta\omega \cdot t_D. \quad (9)$$

Here $\tau$ is the dimensionless time $\tau = t/t_D$. The inner integral in Eq. (8), which is taken over the directions of $\mathbf{q} = \mathbf{k}\rho$, depends exclusively on the object shape. The object size enters Eq. (8) only through the diffusion time $t_D$, Eq. (7). The function $g$ depends on the particular sequence of the radiofrequency (rf) pulses applied to manipulate the spins and is discussed later.

As a conservative estimate, the formal series for $f(t)$ converges when $\alpha < 1$. Odd orders of the expansion in $\alpha$ are imaginary. They renormalize the homogeneous component of the suspension's magnetic susceptibility. Since the first order vanishes the correction to $\omega_L$ is proportional to $\alpha^3$. The signal attenuation is determined by the even orders in $\alpha$. The correction to (8) is of the order of $\alpha^4$ and is negative.

Consider the free induction decay (FID), an evolution after a single rf $\pi/2$ pulse which creates the maximal transverse spin magnetization. The function $g$ in (8), denoted as $g_{\mathrm{FID}}$, is proportional to a time convolution of the three free diffusion propagators $\eta^{(0)}(\mathbf{q}, \tau) = \theta(\tau)e^{-q^2\tau}$, $\theta(\tau)$ being a unit step function (Fig. 1, left):

$$g_{\mathrm{FID}}(q^2\tau) = q^2\tau - 1 + e^{-q^2\tau}. \quad (10)$$

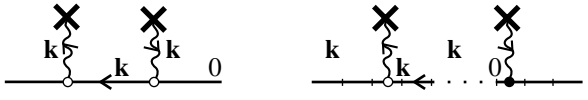


FIG. 1. Second order processes for $f(t)$. Left: FID relaxation. Circles, wavy lines, and crosses stand for $-i\delta\omega$, $Y(\mathbf{k})$, and $\tilde{v}(\mathbf{k})$ respectively. Solid lines represent free propagators $\eta^{(0)}(\mathbf{k}, \tau)$ in time intervals between interactions. External momenta are set to zero due to Eq. (3). Right: CPMG relaxation. Each section represents a free propagator $\eta^{(0)}$ in the interval $\Delta t$ between successive refocusing pulses. Complex conjugation on every other interval $\Delta t$ is indicated with the filled circle. Equation (12) is obtained as a sum of all such configurations.

To reduce sensitivity to large scale field inhomogeneities, samples are often irradiated by a number of refocusing rf $\pi$ pulses. Each such pulse quickly rotates the spins by $\pi$ around an axis which is transverse to $\hat{\mathbf{z}}$. This is equivalent to a complex conjugation of $\eta$ developed up until this time moment. The resulting distribution $\eta^*$ is the initial condition for the further evolution.

In the spin echo (SE) technique [14] a single $\pi$ pulse is applied at the time $t_E/2$ and the signal is measured at $t = t_E$. The corresponding $g$ function reads

$$g_{\mathrm{SE}} = q^2\tau_E - 3 + 4e^{-q^2\tau_E/2} - e^{-q^2\tau_E}, \qquad \tau_E = \frac{t_E}{t_D}. \tag{11}$$

In the CPMG (Carr-Purcell-Meiboom-Gill) protocol [15] refocusing $\pi$ pulses are generated in a long train and the steady state signal is studied as a function of the interpulse interval $\Delta t$ (Fig. 1, right):

$$g_{\mathrm{CPMG}} = q^2\tau - 2\tanh\frac{q^2\tau}{2}, \qquad \tau = \frac{\Delta t}{t_D}. \tag{12}$$

Equations (10)–(12) yield that at $\tau \ll 1$, $f \propto \tau^2$ for the FID and $f \propto \tau^3$ for the SE and the CPMG sequences. Asymptotic expansion of (8) in $\tau^{-1/2}$ at $\tau \gg 1$ gives

$$r_2 \equiv \frac{f(\tau)}{\tau} \simeq \frac{2\pi\alpha^2}{15}\left(\int_0^\infty dq \int \frac{d\hat{\mathbf{q}}}{4\pi} \left|\frac{\tilde{v}(\mathbf{q})}{\tilde{v}(\mathbf{0})}\right|^2 - \frac{A}{\sqrt{\tau}}\right), \tag{13}$$

with $A_{\mathrm{FID}} = \sqrt{\pi}$, $A_{\mathrm{SE}} = (2\sqrt{2}-1)\sqrt{\pi}$, and $A_{\mathrm{CPMG}} = (2\sqrt{2}-1)\zeta(3/2)/\sqrt{\pi} \approx 2.695$ for the considered pulse sequences. The dimensionless NMR relaxivity $r_2$ is shown in Fig. 2, left, for the case of the homogeneously magnetized spherical particles. Shape dependence is illustrated in Fig. 2, right, for the case of disk-shaped objects. The height-to-radius ratio $c$ defines the disk shape, with $c = 0.5$ being close to the intact RBC.

Below we analyze our results, Eqs. (8) and (13).

*(i) Relaxation* (4) *crucially depends on the shape of the object.*—It is the form factor $\tilde{v}(\mathbf{k})$ that governs the convergence of the integral for large $\mathbf{q} = \mathbf{k}\rho$ in (8). The integral converges at $k \sim 1/\rho$, allowing one to probe the object's structure. (A quantum mechanical analogy is scattering amplitude dependence on the form factor of the external potential.) A pointlike magnetization $v \propto \delta(\mathbf{r})$ causes a divergence in Eqs. (8) and (13). In the present case this "nonrenormalizability" (nonuniversal cutoff dependence) effectively increases sensitivity in the NMR measurements.

*(ii) Shape sensitivity is a consequence of a singular interaction* $Y \sim r^{-\nu}$ between nuclear spins and objects. Consider the case when the singularity in $Y$ is cut off at a scale $r < a$. Then $Y(\mathbf{k}) \to 0$ as $ka > 1$. If $a > \rho$, the integral in Eq. (8) is insensitive to the form factor since it converges at $k < 1/a < 1/\rho$, destroying shape sensitivity. Physically, such a cutoff introduces a spherical "cloud" of a radius $a$ around each object. This cloud smears information about the object's structure. The power necessary for shape dependence is $\nu > 2 + (d-2)/N$ for the $N$th order in $d$ dimensions. Thus both magnetic dipole ($\nu = 3$) and contact interaction $Y = \delta(\mathbf{r})$ in $d = 3$ yield shape sensitivity already in the second order, as shown above.

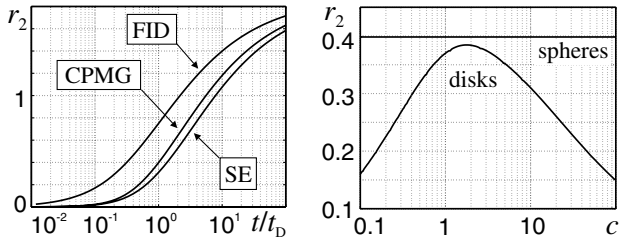


FIG. 2. Mesoscopic relaxivity $r_2 = f(\tau)/\tau$ for $\alpha^2 = 15/2\pi$. Left: objects are spheres, $t = t_E$ for the SE, $t = \Delta t$ for the CPMG. Right: shape effect: disks vs spheres. CPMG relaxivity $r_2(\Delta t/t_D = 1)$, objects are disks with height-to-radius ratio $c$, and spheres of the same volume.

*(iii) Shape sensitivity is present for any field* $B_0$.—Above we demonstrated shape sensitivity in the domain where the perturbative approach is reliable ($\alpha \ll 1$). We now prove it for any $\alpha$. Integrals such as (8) whose convergence is form factor dependent appear in each order of the perturbation series for $f(t)$. Although angular integrations impede explicit summation of this series, they do not cause nonanalyticity at $\alpha = 0$, and thus radius of convergence in $\alpha \propto B_0$ is finite. Therefore the series can be analytically continued to the large field domain $\alpha > 1$ where the perturbation theory formally breaks up. The final result for $f(t)$ would still be form factor dependent, which proves shape sensitivity for *any* field.

*(iv) Shape sensitivity is a generic effect.*—Consider a *diffusion limited chemical reaction* on impurities with a shape $u(\mathbf{r})$. The FID signal analytically continued by $-i\omega(\mathbf{r}) \to u(\mathbf{r})$ gives the impurity shape dependent reaction rate.

Below we compare the results (8) and (13) with experiments. As a first test we use the reported relaxation rate in dilute ($\zeta = 0.02$) suspensions of polystyrene microspheres in paramagnetically doped water [16] (Fig. 3, left).

Further experiments were performed on the deoxygenated blood with a high RBC volume fraction $\zeta = 0.40$–$0.60$ [4–6]. To apply Eqs. (8) and (13) one needs to take into account a slower diffusion inside the cells and to extend our approach for large $\zeta$. The former will be considered elsewhere. For now, we obtain upper and lower estimates for the relaxation rate by using in Eq. (8) the values $D_{\mathrm{in}}$, $D_{\mathrm{out}}$ of the diffusion coefficient in erythrocytes and plasma, respectively.

The $\zeta \sim 1$ case poses a challenging task equivalent to finding the statistical sum of a dense gas of objects. Instead we replace $\zeta$ by $\zeta(1-\zeta)$ in (4), which is well supported experimentally [17]. Such a replacement is justified by the virial expansion. Equation (4) treats

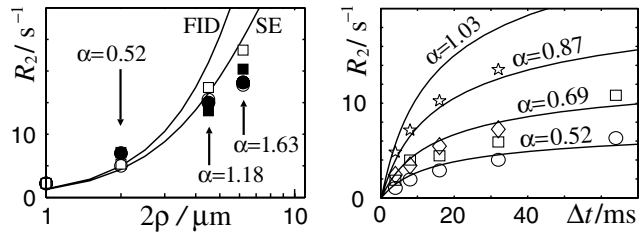


FIG. 3. Theory (lines) vs experiments (symbols). Left: relaxation rate $R_2 = -(\ln s)/t$ for the FID (boxes) and SE (circles) as a function of the particle diameter. Filled and hollow symbols correspond to measured and Monte Carlo simulated relaxation rates [16]. Right: CPMG relaxation rate for the human blood samples [6] for $B_0 =$ 1.41, 1.18, 0.94, 0.71 T (from top to bottom). Experimental errors are 10%–20% [6]. Following our discussion after Eq. (8), theory agrees with experiment for small $\alpha$ and overestimates it for $\alpha \simeq 1$.

exactly the first cumulant of the statistical sum. The second cumulant provides an $\mathcal{O}(\zeta^2)$ *negative* correction. This together with a vanishing mesoscopic contribution as $\zeta \to 1$ justifies a quadratic polynomial interpolation, $\zeta(1-\zeta)$. The latter is correct as $\zeta \to 0$ and 1 and describes a crossover between the dilute and the extremely dense cases.

The relaxation rate in deoxygenated blood measured in [4] quadratically depends on the magnetic field, $-(\ln s)/t = \kappa_1 B_0^2$, in agreement with Eq. (8). The proportionality coefficient $\kappa_1$ was found to be 7.2 s$^{-1}$ T$^{-2}$ for the CPMG pulse sequence with $\Delta t = 4$ ms. In [4], the field range $B_0 = 0.05$–1.5 T yields $\alpha = 0.033$–0.99. We calculated $\zeta = 0.55$ from the parameters given in [4], utilized the magnetic susceptibility of the deoxygenated RBCs $\chi = 2.7 \times 10^{-7}$ [5], and simulated the intact erythrocytes by disks of the known volume of 87 $\mu$m$^3$ with the height-to-radius ratio of $c = 0.5$. Using $D_{\text{out}} =$ 2.20 $\mu$m$^2$/ms and $D_{\text{in}} = 0.76$ $\mu$m$^2$/ms [18], our theory gives $4.7 < \kappa_{1\text{th}} < 5.6$ s$^{-1}$ T$^{-2}$.

To assess this result we note that neither the susceptibility of RBCs nor their actual shape was reported in [4]. Chemicals used to treat the samples are likely to change osmotic pressure in plasma, which would deform the RBCs thus changing all relevant parameters.

Quadratic dependence of the SE blood relaxation rate on $\chi$, which follows from Eq. (8), was confirmed by varying the RBC oxygen saturation $y$ in the field $B_0 =$ 1.5 T [5]: $-(\ln s)/t = \kappa_2(0.95 - y)^2$, with the measured coefficient $\kappa_2 = 55$ s$^{-1}$ for $\zeta = 0.3$ and $\kappa_2 = 59$ s$^{-1}$ for $\zeta = 0.4$. Our approach results in the corresponding ranges $26 < \kappa_{2\text{th}} < 56$ s$^{-1}$ and $30 < \kappa_{2\text{th}} < 64$ s$^{-1}$.

The CPMG relaxation rate $R_2 = -(\ln s)/t$ in the whole blood was measured [6] as a function of the interecho interval (Fig. 3, right) for $0.71 < B_0 < 1.41$ T. We simulated blood as described above using $D = D_{\text{out}}$ for plasma. The use of the value $D_{\text{in}}$ instead of $D_{\text{out}}$ yields about the same rate $R_2$ for the short times and approximately a twofold increase of $R_2$ for the large times.

This brief survey shows that, although crude, our model captures the essential features of the NMR relaxation. Experiments at higher fields [11,12] confirm the shape dependence for $\alpha > 1$. Their results can be well described by adjusting $t_D$ and $\alpha$ [8] or by fitting to a simple chemical exchange model [19]. However, fitting has a predictive power when the signal universally depends on a handful of phenomenological parameters. Shape sensitivity makes such a fitting meaningless in the case of varying tissue structure. Because of the same reason, in experiments analogous to [4–6,11,12] it is essential to control volume fraction, shape, and susceptibility of paramagnetic objects, and effective diffusion coefficient in the sample.

To conclude, we showed that transverse relaxation from a suspension of paramagnetic objects is extremely sensitive to the shape of the individual object. This sensitivity to geometic structure is a generic effect that can be employed as a novel type of contrast in NMR measurements thus effectively increasing spatial resolution.

D. N. appreciates a visiting grant and hospitality of the Section of Medical Physics, University Hospital Freiburg.

*Electronic address: kiselev@ukl.uni-freiburg.de

[1] P. P. Mitra *et al.*, Phys. Rev. Lett. **68**, 3555 (1992).
[2] *Diffusion and Perfusion Magnetic Resonance Imaging*, edited by D. Le Bihan (Raven Press, New York, 1995).
[3] D. A. Yablonskiy *et al.*, Proc. Natl. Acad. Sci. U.S.A. **99**, 3111 (2002).
[4] R. A. Brooks *et al.*, J. Magn. Reson. Imaging **4**, 446 (1995).
[5] W. M. Spees *et al.*, Magn. Reson. Med. **45**, 533 (2001).
[6] J. M. Gomori *et al.*, J. Comput. Assist. Tomogr. **11**, 684 (1987).
[7] D. A. Yablonskiy and E. M. Haacke, Magn. Reson. Med. **32**, 749 (1994).
[8] J. H. Jensen and R. Chandra, Magn. Reson. Med. **44**, 144 (2000).
[9] V. G. Kiselev and S. Posse, Phys. Rev. Lett. **81**, 5696 (1998); **83**, 1487 (1999); Magn. Reson. Med. **41**, 499 (1999).
[10] W. R. Bauer *et al.*, Phys. Rev. Lett. **83**, 4215 (1999).
[11] F. Q. Ye and S. Allen, Magn. Reson. Med. **34**, 713 (1995).
[12] P. Gillis *et al.*, Magn. Reson. Med. **33**, 93 (1995).
[13] H. C. Torrey, Phys. Rev. **104**, 563 (1956).
[14] E. L. Hahn, Phys. Rev. **80**, 580 (1950).
[15] H. Y. Carr and E. M. Purcell, Phys. Rev. **94**, 630 (1954); S. Meiboom and D. Gill, Rev. Sci. Instrum. **29**, 688 (1959).
[16] R. Weisskoff *et al.*, Magn. Reson. Med. **31**, 601 (1994).
[17] K.R. Thulborn *et al.*, Biochim. Biophys. Acta **714**, 265 (1982).
[18] J. G. Li *et al.*, Magn. Reson. Med. **40**, 79 (1998).
[19] R. A. Brooks *et al.*, Magn. Reson. Med. **45**, 1014 (2001).